Mechanical Systems and Signal Processing 98 (2018) 310–323

Contents lists available at ScienceDirect

Mechanical Systems and Signal Processing

journal homepage: www.elsevier.com/locate/ymssp

A sonification algorithm for developing the off-roads models for driving simulators

Veturia Chiroiu [a,*], Cornel Brişan [b], Dan Dumitriu [a], Ligia Munteanu [a]

[a] Institute of Solid Mechanics of Romanian Academy, Dept. of Deformable Media and Ultrasonics, Ctin Mille 15, Bucharest 010141, Romania
[b] Technical University of Cluj-Napoca, Faculty of Mechanics, Dept. of Mechatronics and Machine Dynamics, str. Memorandumului nr.28, Cluj-Napoca 400114, Romania

ARTICLE INFO

Article history:
Received 16 October 2016
Received in revised form 11 March 2017
Accepted 3 May 2017
Available online 10 May 2017

Keywords:
Off-road models
Driving simulators
Sonification
Polynomial chaos expansion

ABSTRACT

In this paper, a sonification algorithm for developing the off-road models for driving simulators, is proposed. The aim of this algorithm is to overcome difficulties of heuristics identification which are best suited to a particular off-road profile built by measurements. The sonification algorithm is based on the stochastic polynomial chaos analysis suitable in solving equations with random input data. The fluctuations are generated by incomplete measurements leading to inhomogeneities of the cross-sectional curves of off-roads before and after deformation, the unstable contact between the tire and the road and the unreal distribution of contact and friction forces in the unknown contact domains. The approach is exercised on two particular problems and results compare favorably to existing analytical and numerical solutions. The sonification technique represents a useful multiscale analysis able to build a low-cost virtual reality environment with increased degrees of realism for driving simulators and higher user flexibility.

1. Introduction

Recently, substantial progress was made in solving nonlinear equations with random input data defined by its mean and correlation function [34,24]. The off-roads models for driving simulators can be viewed as constraint satisfaction problems in which the sonification algorithms may repeatedly assigns values to variables, terminating when all constraints are satisfied. In this paper we suggest a version of the sonification algorithm based to the stochastic polynomial chaos analysis for solving the 3D normal contact problem with friction for off-roads driving simulators [32,7,41]. The aim is to overcome the difficulties of identification of unsatisfied constraints for a particular off-road profile. The randomly character of the stiffness and damping in the contact interfaces, due to vibro-impacts and frictional slips hampers developing the off-road models for driving simulators [25,43,19,12,3]. It is known that, the friction model changes the characteristics of the vibro-impact phenomenon in terms of duration, dissipation of energy, accelerations and decelerations. In turn, the vibro-impact dynamics changes the friction pattern by the appearance of the micro-slips consisting of elastic and plastic deformation [15,22,31,23]. The sonification algorithm comes to solve these problems by treating the random fields as elements of Hilbert space [30,16,38]. The unknown coefficients in the polynomial chaos expansion are identified by using a genetic algorithm. The sonification algorithm uses the geometric properties of hardly detectable details of the real off-roads and random properties of different

* Corresponding author.
E-mail addresses: veturiachiroiu@yahoo.com (V. Chiroiu), Cornel.Brisan@mmfm.utcluj.ro (C. Brişan), dumitri04@yahoo.com (D. Dumitriu), ligia_munteanu@hotmail.com (L. Munteanu).

http://dx.doi.org/10.1016/j.ymssp.2017.05.002
0888-3270/

cross-sectional slices of images furnished by the transformation map [25,27,36]. For existing data for shape and curvature, it is important to discover of more or less hidden information in what concerns the contact tire/off-road, to help the performance of the developed algorithms [4,11,17,39].

The scheme of contact between the tire and the off-road is represented in Fig. 1, where F_c is the contact force, F_{tx} the longitudinal component of the friction force acting in the X direction, F_{ty} the lateral component of the friction force acting in the Y direction, and α the angle between the direction X and the direction of travel.

We will focus in this paper on the evaluation of the off-road models related to the sonification algorithms and polynomial chaos expansion technique, which were not done previously in the literature.

The paper is organized as follows: Section 2 is devoted to the formulation of 3D normal contact problem with random contact domains. In Section 3, the polynomial chaos expansion of the solutions is presented together to the probabilistic collocation method to find the unknown parameters. Results are reported in Section 4. Comparisons to existing analytical and numerical solutions are provided by Section 5, while some Conclusions are drawn in Section 6.

2. The 3D normal vibro-contact problem

This Section describes a virtual experiment concerning driving on off-roads designated to build an off-road simulator. The tire tread is modeled as an elastic half-space [32]. The model of the contact tire/road is displayed in Fig.2.

The random contact domain is denoted by D_c, and (ξ, η) coordinates describe points within D_c, P_0 is the total load applied to the tire, and $h_s(X,Y)$, $h_t(X,Y)$, $\Delta(X,Y)$ are the height of the road surface, the height of the tire and the total penetration between the elastic half-space and the road surface, respectively, linked to δ_z by

$$\delta_z = h_t - h_s - \Delta. \tag{2.1}$$

The normal contact pressure $p(\xi, \eta, t)$, the tangential loading in the positive X-direction $q_X(\xi, \eta, t)$, and the tangential loading in the positive Y-direction $q_Y(\xi, \eta, t)$ on the tire, are given by

$$p = p(\xi,\eta)\delta(\xi)\delta(\eta)\exp(i\omega t), \quad q_X = q_X(\xi,\eta)\delta(\xi)\delta(\eta)\exp(i\omega t), \quad q_Y = q_Y(\xi,\eta)\delta(\xi)\delta(\eta)\exp(i\omega t), \tag{2.2}$$

where $\delta(\cdot)$ is the Dirac delta function. The normal contact between the tire and the road is described by Boussinesq equations [8,10,26]

$$\delta_x(X,Y) == \iint_D \frac{p(\xi,\eta)(X-\xi)(1-\nu^2)}{\pi E((x-\xi)^2+(y-\eta)^2)} d\xi d\eta \text{ in } D, \tag{2.3}$$

$$\delta_y(X,Y) == \iint_D \frac{p(\xi,\eta)(Y-\eta)(1-\nu^2)}{\pi E((x-\xi)^2+(y-\eta)^2)} d\xi d\eta \text{ in } D, \tag{2.4}$$

$$\delta_z(X,Y) == \iint_D \frac{p(\xi,\eta)(1-\nu^2)}{\pi E\sqrt{(x-\xi)^2+(y-\eta)^2}} d\xi d\eta \text{ in } D, \tag{2.5}$$

The equilibrium condition is

$$-P_0 = \iint_D p(\xi,\eta) d\xi d\eta. \tag{2.6}$$

Let us introduce the notations: δ_x, δ_y, δ_z the tire-tread displacements due to the normal load only, D the surface of half-space, E the Young's modulus of the half-space and ν the Poisson's ration of the half-space, P is the total load applied to the tire, h_s the height of the road surface, h_t the height of the tire, Δ the total penetration between the elastic half-space and the

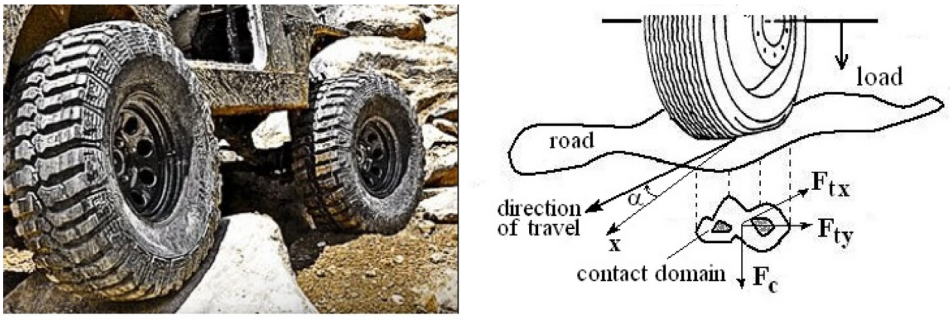

Fig. 1. Scheme of the contact tire/off-road.

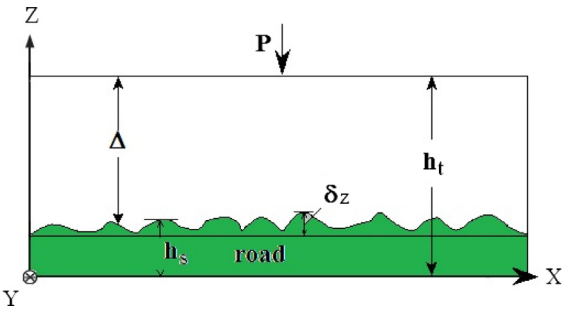

Fig. 2. Model of the contact tire/road.

road surface, and $\bar{D}_c$ the non-contact area, respectively. By denoting with $s(X,Y)$ an arbitrary curve which describe the geometry of any cross-sectional slice of the road, the unilateral contact conditions which describe the non-penetration and the separation outside the contact area are given by

$$\delta_z = h_s - h_t - \Delta,\ p > 0 \text{ contact, for } (X,Y) \in s(X,Y) \subset D_c, \tag{2.7}$$

$$\delta_z > h_s - h_t - \Delta,\ p = 0 \text{ separation, for } (X,Y) \in s(X,Y) \subset \bar{D}_c, \tag{2.8}$$

where (X,Y) describe any surface points, whether inside or outside the contact domain D_c. The contact force is

$$F_c = k\delta_z^n + \tilde{b}\delta_z^p\dot{\delta}_z^q = -\int_A p(\xi,\eta)\mathrm{d}A, \tag{2.9}$$

where A is random area of the contact domain.

For describing the tangential contact between the tire and the road, we add to (2.3)(2.9) the tire-tread displacements $\delta_{xt_x}(X,Y)$, $\delta_{yt_x}(X,Y)$, $\delta_{zt_x}(X,Y)$ due to the tangential loading $q_X(\xi,\eta)$ in the positive X-direction

$$\delta_{xt_x} = \iint_D \frac{q_X(1-\nu^2)}{\pi E\sqrt{(x-\xi)^2+(y-\eta)^2}}\mathrm{d}\xi\mathrm{d}\eta + \iint_D \frac{q_X(X-\xi)^2(1-\nu^2)}{\pi E((x-\xi)^2+(y-\eta)^2)\sqrt{(x-\xi)^2+(y-\eta)^2}}\mathrm{d}\xi\mathrm{d}\eta,\ \text{in } D, \tag{2.10}$$

$$\delta_{yt_x} = \iint_D \frac{q_X(X-\xi)(Y-\eta)(1-\nu^2)}{\pi E((x-\xi)^2+(y-\eta)^2)\sqrt{(x-\xi)^2+(y-\eta)^2}}\mathrm{d}\xi\mathrm{d}\eta \text{ in } D, \tag{2.11}$$

$$\delta_{zt_x} = \iint_D \frac{q_X(X-\xi)(1-\nu^2)}{\pi E((x-\xi)^2+(y-\eta)^2)}\mathrm{d}\xi\mathrm{d}\eta \text{ in } D. \tag{2.12}$$

The friction force due to the tangential loading $q_X(\xi,\eta)$ in the positive X-direction is given by

$$F_{t_x} = k_{t_x}\delta_{xt_x} = -\int_A q_X(\xi,\eta)\mathrm{d}A. \tag{2.13}$$

where δ_{xt_x} is the tangential component of displacement at the contact point due to the tangential loading $q_X(\xi,\eta)$ in the positive X-direction, and k_{t_x} is the tangential stiffness in the X-direction.

Similar relations can be added to (2.3)(2.13) for tire-tread displacements δ_{xt_y}, δ_{yt_y}, δ_{zt_y} due to the tangential loading $q_Y(\xi,\eta)$ in the positive Y-direction. These displacements satisfy the far-field boundary conditions on the half-space [8]. In a similar way, the friction force due to the tangential loading $q_Y(\xi,\eta)$ in the positive Y-direction is given by

$$F_{t_y} = k_{t_y}\delta_{xt_y} = -\int_A q_Y(\xi,\eta)\mathrm{d}A, \tag{2.14}$$

where δ_{xt_y} is the tangential component of displacement at the contact point due to the tangential loading $q_Y(\xi,\eta)$ in the positive Y-direction, and k_{t_y} is the tangential stiffness in the Y-direction. The tangential stiffnesses k_{t_x} and k_{t_y} are determined from

$$k_{tx} = 8a\mu_0, \quad k_{ty} = 8b\mu_0, \tag{2.15}$$

with a, b the radii of the oval shape, while μ_0 is the composite shear modulus given by

$$\mu_0 = \left(\frac{(2-\nu_t)}{\mu_t} + \frac{(2-\nu_r)}{\mu_r}\right)^{-1}, \tag{2.16}$$

where μ_t, μ_r are the shear moduli, and ν_t, ν_r, the Poisson's ratios of the tire and the road, respectively [13].

Functions h_s, h_t and Δ from unilateral contact conditions (2.7) and (2.8) describe the non-penetration and the separation outside the contact area, respectively, and are determined from the road geometry.

When the tire tread and the road are not in contact, the harmonic forces are given by

$$f_t = A_t \exp(i\omega t),\ f_r = A_r \exp(i\omega t). \tag{2.17}$$

They cause undamped harmonic responses

$$\delta_t = B_t \exp(i\omega t),\ \delta_r = B_r \exp(i\omega t), \tag{2.18}$$

or viceversa. Indices t and r refer to the tire and road, respectively, A is the harmonic force amplitude, and B is the displacement amplitude.

When the tire and road are in contact and vibrate harmonically at angular frequency ω, the continuity requires $\delta_t = \delta_r$, and the equilibrium condition $f_t + f_r = 0$ give the following equation of the natural frequencies of the tire in ground contact

$$\frac{\delta_t}{f_t} + \frac{\delta_r}{f_r} = 0,\ \text{or}\ \frac{B_t}{A_t} + \frac{B_r}{A_r} = 0. \tag{2.19}$$

The suspension of the vehicle with two symmetric axes are modeled by the following seven equations of motion written for the sprung mass m that can translate and rotate exhibiting angular oscillations around the mass center, and the masses m_j of the tires B_j, $j = 1,2,3,4$ [35,41,42]

$$m\ddot{z}_1 + \sum_j c_j \Delta_j + \sum_j k_j \dot{\Delta}_j = F_a^3, \tag{2.20}$$

$$m_j \ddot{z}_j + c_j' z_j + k_j' \dot{z}_j - c_j \Delta_j - k_j \dot{\Delta}_j = g_j,\ j = 2,3,4,5, \tag{2.21}$$

$$A\ddot{\alpha} + \sum_j b_j c_j \Delta_j + \sum_j b_j k_j \dot{\Delta}_j = M_1, \tag{2.22}$$

$$B\ddot{\beta} - \sum_j a_j c_j \Delta_j - \sum_j a_j k_j \dot{\Delta}_j = M_2, \tag{2.23}$$

where c_j' and k_j', $j = 1,2,3,4$, are stiffness and damping coefficients of the tires B_j, M_1 and M_2 are the moments acting on the mass m with respect to the mass center, and A, B are the principal central inertial moments. Angles α, $0 \leqslant \alpha \leqslant \pi/2$, and β, $-\pi \leqslant \beta \leqslant \pi$, are relative angular displacements of mass center having the directions OX and OY.

Forces g_j, $j = 1,2,3,4$, acting on the tires are given by

$$g_j = c_j' s_j + k_j' \dot{s}_j, \quad j = 1,2,3,4, \tag{2.24}$$

with $s_j(t)$, $j = 1,2,3,4$, displacement functions furnished by the sonification technique. The $F = -mgk_3$ is the weight of the car, $F_a = F_a^1 i_1 + F_a^3 i_3$ $F_a^2 = 0$ are the aerodynamic force applied on the mass center.

The boundary conditions attached to the tires can be written as

$$\tilde{M}_j = z_0 F_{fj}, \quad F_{shj} = F_{cj} - F_z, \quad j = 1,2,3,4, \tag{2.25}$$

where $\tilde{M}_j$ are the bending moment of B_j corresponding to contact domain D_c, F_z is the vertical load acting on B_j, and F_{sh} is the shearing force in B_j, respectively. The moments $\tilde{M}_j$ are equal to the couple moments created by the friction force F_{fj}, $j = 1,2,3,4$.

The random contact is treated using a particular identifier by checking the minimum distance between bodies [22,25]

$$\min\left(\frac{1}{2}(r_1 - r_2)^T (r_1 - r_2)\right), \quad f_1(r_1) \leqslant 0, \quad f_2(r_2) \leqslant 0, \tag{2.26}$$

where r_1 and r_2 are the position vectors of two points belonging to the tire and the road, respectively, and f_1 and f_2 are bounding surface constraints. The interference distance is defined as

$$\min(-d), \quad f_1(r_1) \leqslant -\frac{d}{2} e_1, \quad f_2(r_2) \leqslant -\frac{d}{2} e_2, \tag{2.27}$$

where d is the interference distance and e_1 and e_2 are the unit vectors.

The random properties of locations is expressed in terms of d. The random shape of the contact is expressed in terms of the half of the contact length a, half of the contact width b (radii of the oval shape are depending of time), and n the power of a superellipse defined by a Lamé curve [14,9,7,33]

$$\left(\frac{x}{a(t)}\right)^n + \left(\frac{y}{b(t)}\right)^n = 1, n > 0, \tag{2.28}$$

where x and y define the envelope of the contact area. The case of $n = 2/3$ corresponds to a squashed astroid, $n = 1$ to a squashed diamond, $n = 2$ to ellipse and $n \to \infty$ to rectangles. The advantage of the Lamé curve consists in the effect of n to rounding the sharp corners. It provides a smooth transition between the oval and the rectangle shape. An examination of (2.26)(2.28) revels that, the response statistics for contact domains of both location and shape, may depend on random properties of the entire car.

The parametric representation of (2.28) is

$$x(t) = a(t)\cos^{2/n}\theta, \quad y(t) = b(t)\sin^{2/n}\theta. \tag{2.29}$$

For area of the ellipsoid (2.28), we find

$$A(t) = 4b\int_0^a \left(1 - \left(\frac{x}{a}\right)^n\right)^{1/n} dx = \frac{4^{1-1/n}a(t)b(t)\sqrt{\pi}\Gamma\left(1+\frac{1}{n}\right)}{\Gamma\left(\frac{1}{2}+\frac{1}{n}\right)}, \tag{2.30}$$

where Γ is the Gamma function $\Gamma(z) = \lim_{n\to\infty}\frac{n!n^z}{z(z+1)\ldots(z+n)}$, $(z \neq 0, -1, -2, \ldots)$.

In what concerns the contact forces, we consider that they act in a continuous manner during the impact, and thus, the analysis is performed by adding the contact forces to the equations of motion [20,21]. Different models have been postulated in time to represent the contact force of two contacting bodies [18,37,2,6].

We consider the Hunt and Crossley [18] model in defining the contact force

$$F_c = k\delta^{\tilde{n}} + \tilde{b}\delta^p\dot{\delta}^q, \tag{2.31}$$

where $\tilde{n}, p, q$ are constants, coefficient k depends on the material and the geometric properties of the bodies in contact, and $\tilde{b}$ is defined with respect to the coefficient of restitution $0 \leqslant e \leqslant 1$. These coefficients are calculated based on the viscoelastic theory. Standard values are $p = n$ and $q = 1$. In the case of central impact between two bodies, the coefficient of restitution is $e = 1 - 2\tilde{b}\dot{\delta}_0/3k$ [22,40]. For $\tilde{b} = 0$, (2.31) reduces to the Hertz model.

In this paper, we consider that the friction F_t occurring at the contact point during sticking can be defined as [21]

$$F_t = k_t\delta_t, \tag{2.32}$$

where δ_t is the tangential component of the tire-tread displacement at the contact point, due to the tangential loadings, and k_t is the tangential stiffness which is determined by the geometry and the material of the contacting objects. For static oblique elastic contact between a tire modeled as a rigid cylinder and a roughly half-space, k_t is estimated to be $k_t = \upsilon|F_c|/\delta$ where $\upsilon = 0.79$ [29].

The boundary conditions (2.25) are modeled as a lognormal random field given by

$$K(s_j, d, D_c, F_c, F_f, x, t) = \exp(Y(x, t), \tag{2.33}$$

where x is the spatial coordinate, $Y(x,t)$ is a Gaussian random field with mean $\langle Y\rangle = 0$ and a prescribed correlation function $C_Y(x,y)$ defined with respect to the variance σ_Y^2 and the correlation lengths of the random field Y

$$C_Y(x,y) = \sigma_Y^2\exp\left(-\frac{|x_1 - y_1|}{\eta_1} - \frac{|x_2 - y_2|}{\eta_2} - \frac{|x_3 - y_3|}{\eta_3}\right). \tag{2.34}$$

3. Polynomial chaos expansion

The images chosen for sonification depict abrupt changes in profile and can benefit from the accompanying sound by calculating of several cross-sectional slices of them, or even by providing additionally information to that gained from images alone. Through sonification, sounds are generated directly from digital images, possible in a bijective way, and tested to see whether they aid in the study of them, or not. Cross-sectional slices of the image can be built by interpolating the sound parameters furnished by the transformation map [7,41].

Consider the set $D\{d_i(t),\ i = 1, \ldots, M\}$ of sound parameters obtained by applying the sonification operator S to a given off-road

$$D = S(p, t), \tag{3.1}$$

where $S(p,t):\ \Omega_1 \times T_0 \to \Omega_2 \times T_0$ is a nonlinear differentiable operator, and Ω_1, Ω_2 are open and bounded subset of R^n. Ω_1 is an open bounded subset of R^n representing the set of image data, and Ω_2 is an open bounded subset of R^n representing the set of sound data, and T_0 the working interval of time.

Consider the inverse nonlinear ill-posed operator equation

$$S^{-1}(D) = s, \tag{3.2}$$

where $S^{-1}(D):\ \Omega_2\times T_0\to\Omega_1\times T_0$, and $s(x,t)$ (i.e. $s_1(Z,X,t)$ or $s_2(Y,X,t)$) is the curve of the cross-sectional slice of the image. Suppose that (3.2) has at least one solution $s\{p_i,t,\ i=1,\dots,p_1\}$.

Let us approximate the solutions $z_j, j=1,2,3,4,5$ and α,β of Eqs. (2.20)(2.25) through the polynomial chaos expansion [45,34]

$$\theta_k(t)=\sum_{i_1=1}^{\infty}a_{i_1k}\Gamma_{1k}(\xi_{i_1k}(t))+\sum_{i_1=1}^{\infty}\sum_{i_2=1}^{i_1}a_{i_1i_2k}\Gamma_{2k}(\xi_{i_1k}(t),\xi_{i_2k}(t))+\sum_{i_1=1}^{\infty}\sum_{i_2=1}^{i_1}\sum_{i_3=1}^{i_2}a_{i_1i_2i_3k}\Gamma_{3k}(\xi_{i_1k}(t),\xi_{i_2k}(t),\xi_{i_3k}(t))+\dots$$
$$k=1,2,\dots,7, \tag{3.3}$$

where $\xi_{i_1}(t),\xi_{i_2}(t),\dots,\xi_{i_d}(t)$ is a set of standard Gaussian random vectors with independent components, and $\Gamma_d(\xi_{i_1}(t),\xi_{i_2}(t),\dots,\xi_{i_d}(t))$ is a Hermite orthogonal polynomial of order d_G given by

$$\Gamma_{d_G}(\xi)=(-1)^{d_G}\exp(\xi^T\xi/2)\frac{\partial^{d_G}}{\partial\xi_{i_1}\dots\xi_{i_d}}(\exp(\xi^T\xi/2)), \tag{3.4}$$

where $\xi=(\xi_{i_1}(t),\xi_{i_2}(t),\dots,\xi_{i_d}(t))$.The 2D (X,Y) cross-sectional slice of the virtual off-road, before and after deformation, are delimitated by two plane curve $s_1(Z,X,t)$ and $s_2(Y,X,t)$ that can be represented also as polynomial chaos expansion

$$s_l(x,t)=\sum_{i_1=1}^{\infty}a_{i_1l}(x)\Gamma_{1l}(\xi_{i_1l}(t))+\sum_{i_1=1}^{\infty}\sum_{i_2=1}^{i_1}a_{i_1i_2l}(x)\Gamma_{2l}(\xi_{i_1k}(t),\xi_{i_2l}(t))+\sum_{i_1=1}^{\infty}\sum_{i_2=1}^{i_1}\sum_{i_3=1}^{i_2}a_{i_1i_2i_3l}(x)\Gamma_{3l}(\xi_{i_1l}(t),\xi_{i_2l}(t),\xi_{i_3l}(t))+\dots\quad l=1,2. \tag{3.5}$$

In practice, we use a finite number of terms, so that the expansions (3.3) and (3.5) can be approximated by retaining the first P terms, respectively,

$$\theta_k(t)=\sum_{j=1}^{P}b_{jk}\Psi_{jk}(\xi(t)),\quad k=1,2,\dots,7, \tag{3.6}$$

$$s_l(x,t)=\sum_{j=1}^{P}c_{jl}(x)\Psi_{jl}(\xi(t)),\quad l=1,2, \tag{3.7}$$

where ξ is a vector of dimension N. There is a one-to-one correspondence between the (3.3), (3.5) and (3.6), (3.7). The total number P is calculated from [34]

$$P=\frac{(N+d_G)!}{N!d_G!}. \tag{3.8}$$

The unknown parameters b_{jk}, the functions $c_{jl}(x)$, and the coefficients c'_m and k'_m, $m=1,2,3,4$, which appear in (2.24),

$$P=\{b_{jk},c_{jl}(x),c'_m,k'_m\},\ j=1,2,\dots,P,\ k=1,2,\dots,7,\ l=1,2,\ m=1,2,3,4, \tag{3.9}$$

are find by the probabilistic collocation method [44].

4. Results

In this section the results of applying the sonification algorithm for developing irregular off-road profiles are presented. Recall that the forces $g_j, j=1,2,3,4$, acting on the tires given by (2.24) with $s_j(t), j=1,2,3,4$, displacement functions are furnished by the sonification technique.

We solve the problem for off-roads involving asperities of higher scale, usually between 1 and 15 cm. A cross-sectional slice (Z,X) of the off-road is displayed in Fig. 3a, while Fig. 3b shows some rocks with a total height of 15 cm [32].

The direction of travel is OX, while the depth of the road is OZ. Possible 2D (X,Y) cross-sectional slice of this virtual off-road, before and after deformation, are delimitated by two plane curve $s_1(Z,X)$ and $s_2(Y,X)$ that can be represented as series of cnoidal functions

$$s_1(Z,X)=\sum_{j=1}^{N}\alpha_j\mathrm{cn}^j(m_j,k_{1j}X+k_{3j}Z),\ s_2(Y,X)=\sum_{j=1}^{N}\beta_j\mathrm{cn}^j(m_j,k_{1j}X+k_{2j}Y), \tag{4.1}$$

where N is the finite number of degrees of freedom of the curves, $0\leqslant m_j\leqslant 1$ is the modulus of the Jacobean elliptic function, and α,β,k are unknown parameters that are determined from an inverse technique.

The representations (4.1) suggest that the sonification method is a generalization of Fourier series with cnoidal functions as fundamental basis functions. The advantages of sonification with respect to a standard Fourier transform approach in obtaining the asperity spectrum, consists in accuracy in capturing the hidden information on the surface shape and curva-

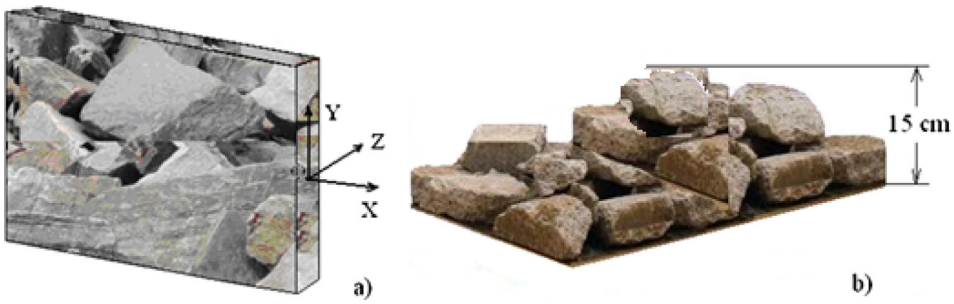

Fig. 3. (a) A 3D sample of the virtual off-road; (b) The layer of rocks [32].

ture. This is because the cnoidal functions are much richer than the trigonometric or hyperbolic functions, that is, the modulus m of the cnoidal function, $0 \leqslant m \leqslant 1$, can be varied to obtain a sine or cosine function ($m \cong 0$), a Stokes function ($m \cong 0.5$) or a solitonic function, sech or tanh ($m \cong 1$).

The 2D cross-sectional road slices delimitated by plane curves $s(Z,X)$ are built as series of cnoidal functions, before and after deformation.

The following parameters are selected: $m = 1500$ kg, $m_1 = m_2 = 40$ kg, $m_3 = m_4 = 40$ kg, $k_i' = 250$ kN/m, $c_i' = 0.6$ kN/m, $i = 1,2,3,4$, $k^h = 20$ kN/m, $k^s = 12$ kN/m, $c^h = 5$ kNs/m, $c^s = 0.5$ kNs/m. Other parameters: $\nu_t = 0.49$, $E_t = 5.6$ MPa, $\mu_t = 20$ MPa for the tire, and $\nu_r = 0.4$, $E_r = 1.92$ MPa, $\mu_r = 0.5$ MPa for the gravelly soil, respectively.

The identification of contact patches in the interval T_0 is performed by checking the minimum distance between bodies according to (2.26) and (2.27). As result, for a speed of the vehicle of 10 m/s, a number of more than 500 contact points were detected in the given interval of time $t \in T_0 = [0; 5\ \text{s}]$. By defining a contact patch consisting from a minimum nearest 5 contact points, a number of more than 100 contact patches were identified.

The boundary conditions (2.25) are modeled as a lognormal random field (2.33) with correlation length $\eta_1 = \eta_2 = 3.0$ and spatial variability $\sigma_Y = 1.0$ for the random field $Y(x,t)$. The expansion was taken with $N = 5$ and $P = 11$.

In the case of uncertain boundary conditions, unknowns b_{jk}, $c_{jl}(x)$, c_m' and k_m', $m = 1,2,3,4$, which appear in (3.9) are assumed uncertain and their evaluation is made by the probabilistic collocation method. The solutions z_j, $j = 1,2,\ldots,5$, of the Eqs. (2.20)(2.23), play the role of random variables in this evaluation. The standard $k-\varepsilon$ solution is used as initial solution. The density functions $p_j(x), j = 1,2,\ldots,5$, of solutions $z_j, j = 1,2,\ldots,5$, are assumed known. The mean value of the solutions $z_j, j = 1,2,\ldots,5$, are calculated as $\int_{-\infty}^{\infty} z_j p_j(x)\mathrm{d}x$. The mean value of z_1 is presented in Fig. 4 as function of x on $[0,L]$ at fixed value $y = 4$. The collocation method is compared against the Monte Carlo results. The variance of solutions and comparison of the Monte Carlo and probabilistic collocation method, is presented in Fig. 5.

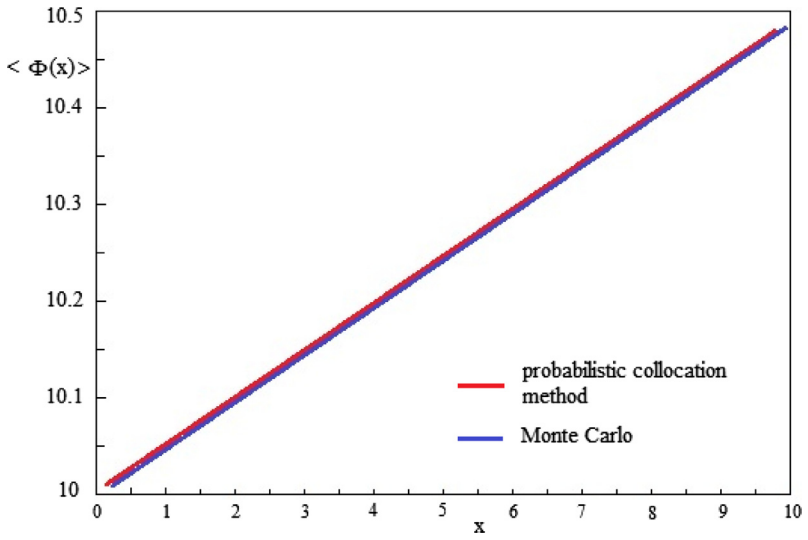

Fig. 4. The average of the solution z_1: comparison of the Monte Carlo and the probabilistic collocation method.

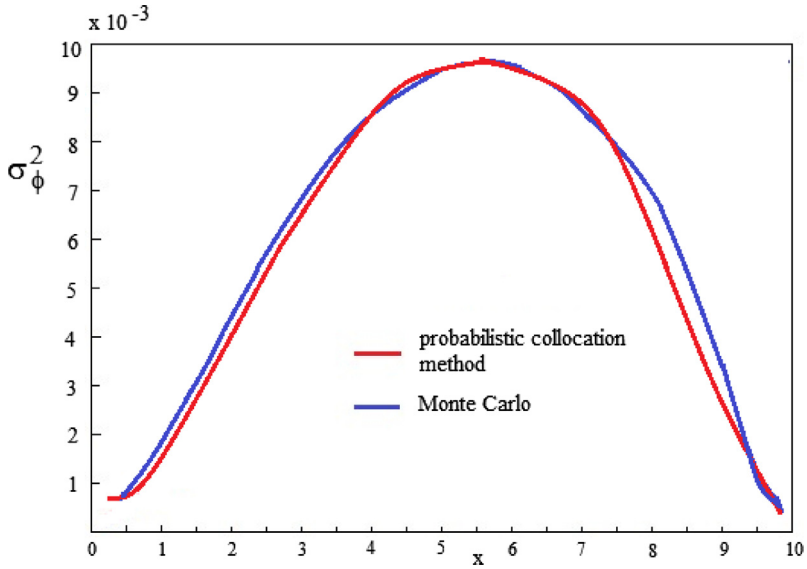

Fig. 5. The variance of the solution z_1: comparison of the Monte Carlo and the probabilistic collocation method.

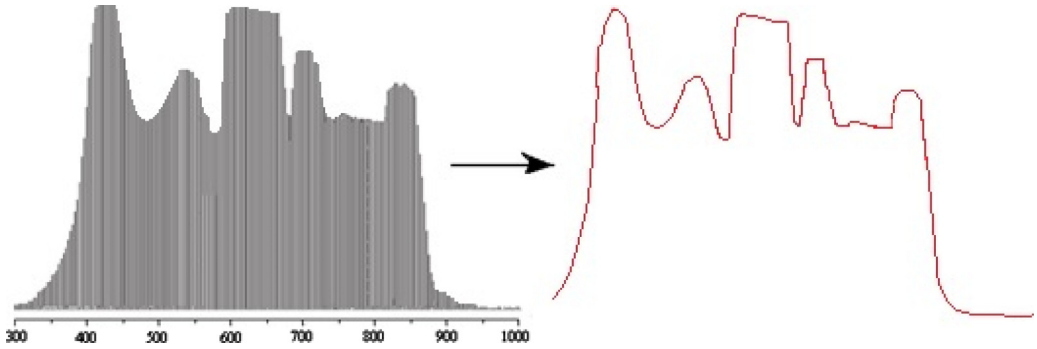

Fig. 6. Spectra of the cross sectional slice (Z,X), and the corresponding curve $s(Z,X)$ before deformation.

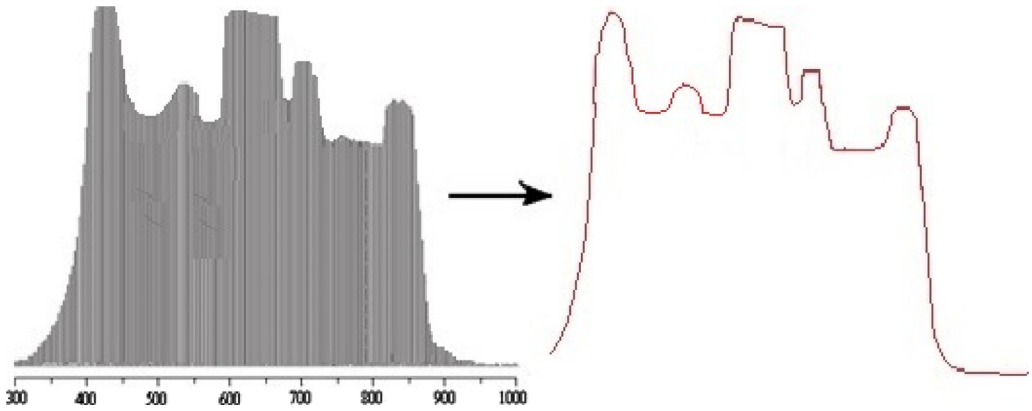

Fig. 7. Spectra of the cross sectional slice (Z,X), and the corresponding curve $s(Z,X)$ after deformation.

For the cross-sectional slice (Z,X) of the off-road, the spectra plotted data is represented in the left-hand side of Fig. 6, before deformation of the road. Each spectrometer pixel is in the range 300–1000 nm, with 3.125 nm wide. The absolute amplitudes between plots are not significant. In the right-hand side of Fig. 6, the corresponding curve $s(Z,X)$ before

deformation is represented. Fig. 7 represents both the spectra plotted data and the corresponding curve $s(Z,X)$ after deformation of the road. By comparing Figs. 6 and 7, we notice a slight variation before and after deformation of the road, within the spectra plotted data and the corresponding curve $s(Z,X)$, respectively.

For arbitrary four cross-sectional slices (Z,X) of the off-road, the field of vertical displacements $s_j(t)$, $j=1,2,3,4$ of tires, are represented in Fig. 8. Fig. 8 addresses vertical displacements in the order of one hundred millimetres. To simplify the calculation, the functions s_j, $j=1,2,3,4$ are supposed to be periodically on the horizontal scale, with a period of 3 mm.

The contact domain D_c is modeled as a superellipse shape defined by (2.28). A total of 32–54 contact patches were identified in the interval of time T_0 for vertical loads of 2000, 3000, 5000 and 8000 N, respectively. Dimension a has values between 32.5 mm and 100 mm, and b between 44.2 mm and 76.2 mm, while the exponent n takes values between from 2 to 3.9. The maximum value of the contact pressure for a contact pat ch of each tire, are plotted in Fig. 9 with respect to $2a/a_0$, with a_0 a reference radius. The calculation was carried out for $F_z = 3000$ N. The contact patches of all tires has the following dimensions: $a=42.4$, $b=53.9$, $n=2.4$ for B_1, $a=44.9$, $b=52.3$, $n=2.4$ for B_2, $a=45.7$, $b=53.7$, $n=2.4$ for B_3, and $a=49$, $b=54.3$, $n=2.6$ for B_4, respectively. In addition, the contact forces along the X- and Y-direction, respectively, and the longitudinal and lateral components of the friction forces F_{tx} and F_{ty} were computed in each contact domain.

5. Comparison to existing results

The sonification is a multi-scale dynamic approach based on the 3D normal vibro-contact analysis and identification of the contact patches between tire and road. The road irregularities such as jump bumps, depressions, potholes, slopes, vertical upwards, lane grooves, rough obstacles are extracted from digital images. The sound is generated from images, possible in a bijective way, and tested to see whether they aid in the study of them, or not.

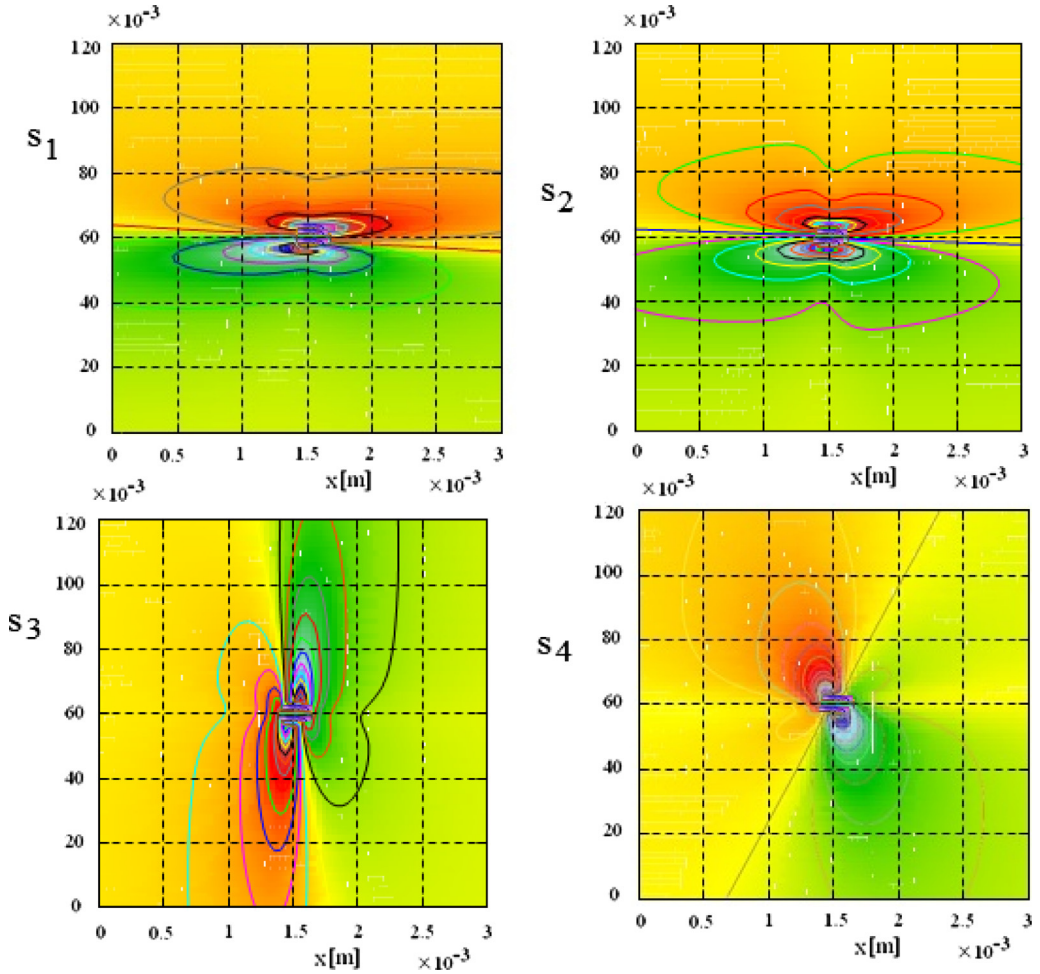

Fig. 8. Field of vertical displacements of tires s_j, $j=1,2,3,4$ in the plane (Z,X).

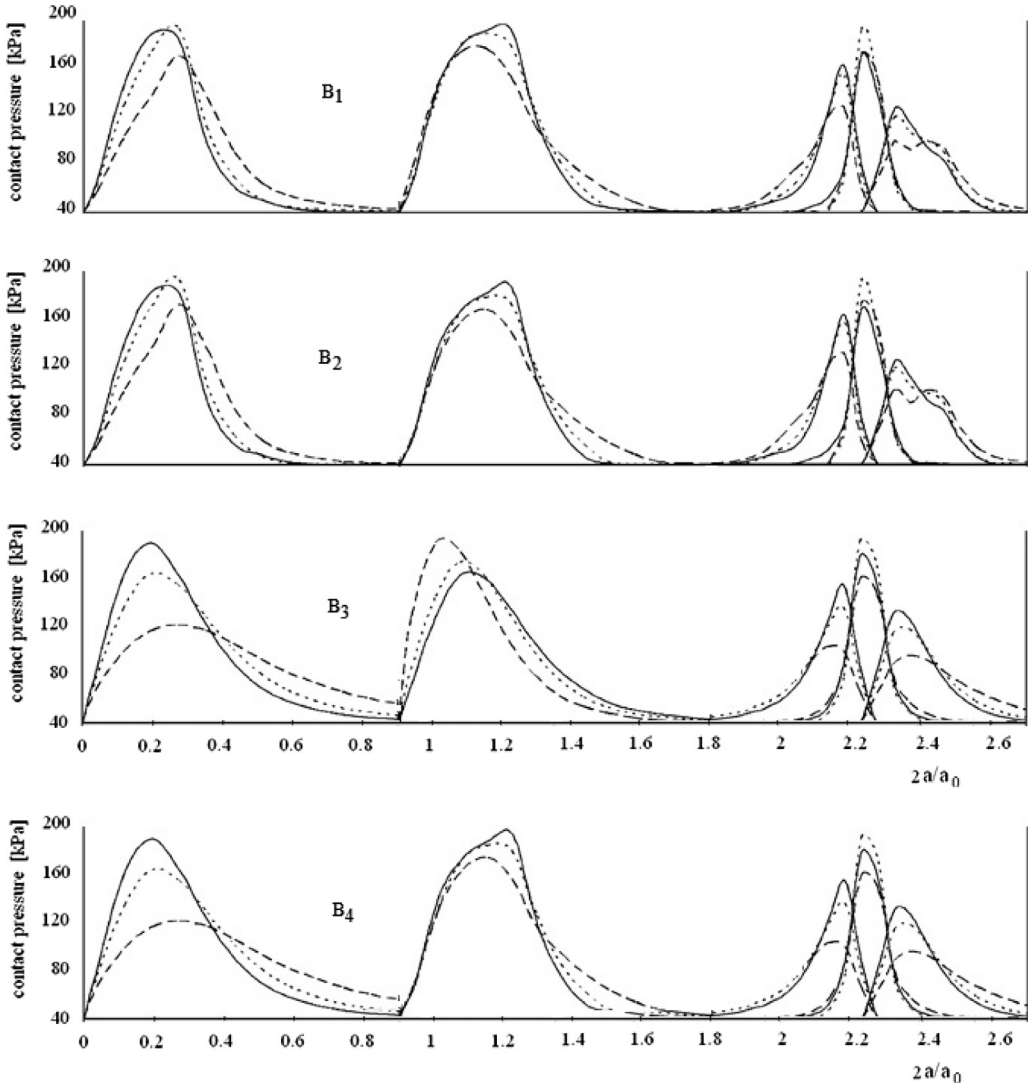

Fig. 9. Maximum contact pressure in tires B_j, $j = 1, 2, 3, 4$ in an arbitrary contact domain.

In order to show the efficiency of the sonification procedure and to verify the correctness of the results, we compare our results with other results from the literature obtained by other methods or by experiments.

Consider firstly, the climbing of a car on an artificial hill [5]. The motion of the car for the same data as B&F is simulated. It is interesting to compare our results regarding the vertical displacements of the masses m_j of the tires obtained from (2.20) (2.25), to the same vertical displacements obtained by B&F. The results are displayed in Fig. 10. The comparison with the B&F results is positive. Our results are in a good agreement with those of B&F, obtained with MBD model and Motion Solve 9.0 and those of Munteanu et al. [32].

Consider next the experiment done to the automotive laboratory of the Mechanical Engineering Faculty, Technische Universiteit Eindhoven with a real car wheel on the flat-plate [1]. The flat-plate has applied a load on the tire under realistic tire/road boundary conditions. For this experiment the Fuji type film was used [28]. The pressure is gradually applied within 5 s. After that the pressure is kept constant for approximately 5 s and next the pressure is released in 5 s. Fig. 11, visualizes the spectra of the cross sectional slice (Z, X), and the corresponding curve before deformation for this experiment. The maximum pressure is 4000 N.

The picture of the tire contact in true color shown in Fig. 12 (photo (4.5) in [1] is used to obtain the curve after deformation, via sonification technique.

We compare the sonification results for a nominally flat counterface to the experimental pressure distribution obtained by Backs [1] and presented in Fig. 13.

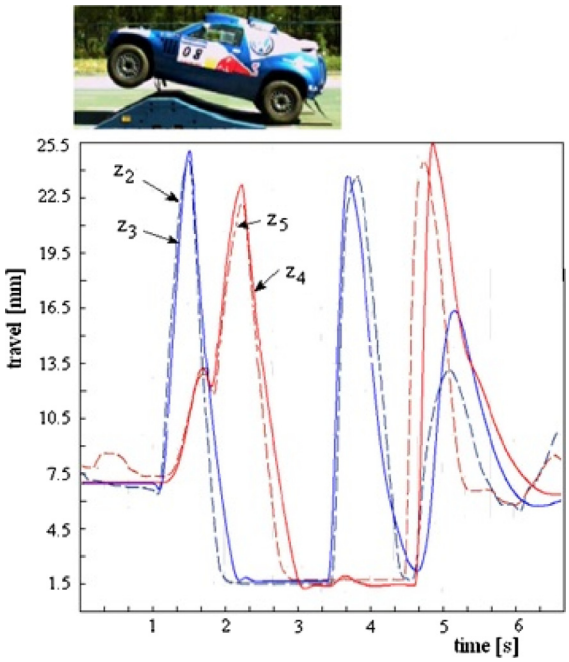

Fig. 10. Vertical displacements of the masses m_j of the tires B_j, $j = 2, 3, 4, 5$ [32].

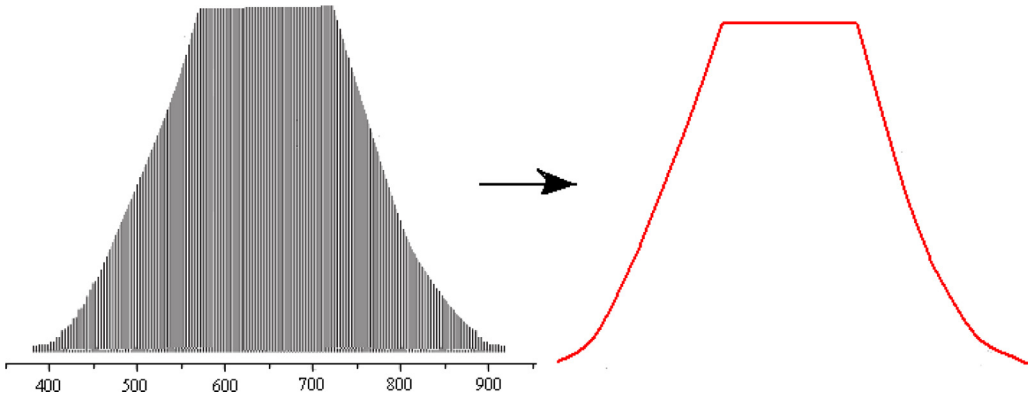

Fig. 11. Spectra of the cross sectional slice (Z, X), and the corresponding curve $s(Z, X)$ before deformation for the real car wheel on the flat-plate.

Maximum value of the contact pressures for this contact patch with respect to $2a/a_0$ are plotted in Fig. 14, where a_0 is one reference radius of the contact domain [32]. The results are in a perfect agreement with the pressure distribution obtained from experiment [1]. In addition, the time evolution of pressure in an arbitrary point of this contact patch is presented in Fig. 15.

The contact path from Fig. 13 was identified by [32] as follows $a = 49.5$, $b = 54.3$, $n = 2.5$ for B_1, $a = 50$, $b = 53$, $n = 2.5$ for B_2, $a = 60.6$, $b = 63.3$, $n = 2.5$ for B_3, and $a = 60$, $b = 60$, $n = 2.7$ for B_4, and $F_z = 3000$ N. In Fig. 14 the maximum contact pressure in this contact patch was computed by [32], in full agreement with data obtained in [1].

The last check is made in this paper (Fig. 15) by computing the evolution in time of the maximum contact pressure in the above-mentioned contact path. The results are confirmed by experimental measurements [1].

6. Conclusions

The aim of this work is to introduce a sonification algorithm based on the stochastic polynomial chaos analysis, for developing the off-road models for driving simulators. The stochastic chaos analysis is suitable to solve 3D vibro-contact problem with friction and uncertain input data. The characterization of a particular stretch of road by total longitudinal, lateral, and

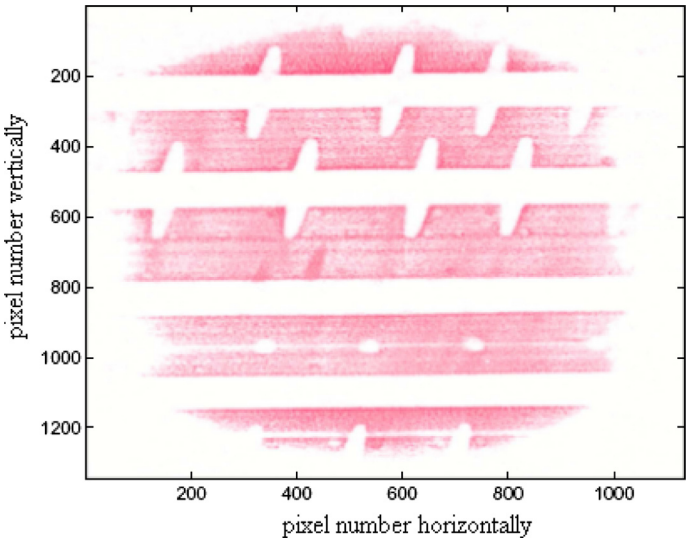

Fig. 12. Tire contact in true color (photo (4.5) in [1]).

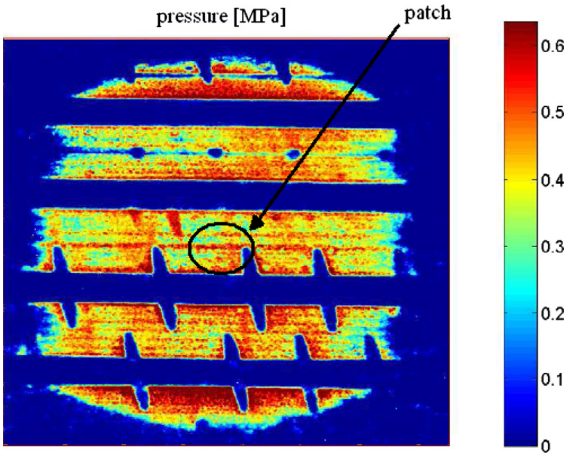

Fig. 13. Experimental pressure distribution and an arbitrary contact patch [1].

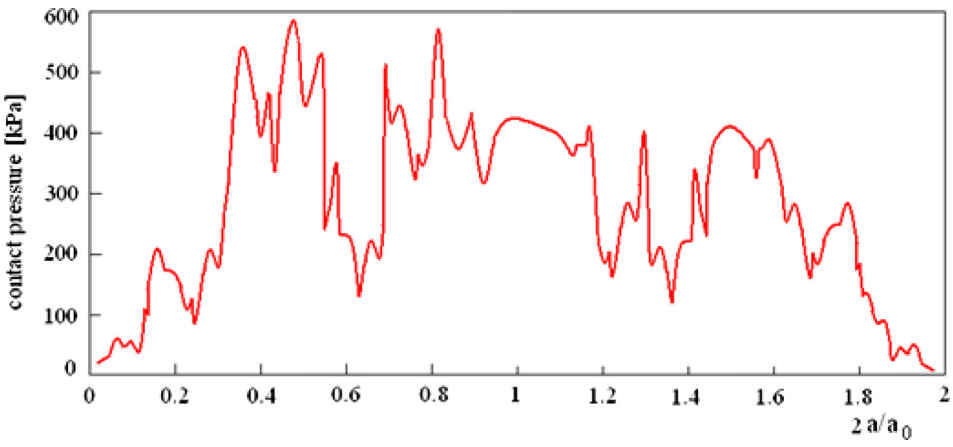

Fig. 14. Maximum contact pressure in the contact patch [32].

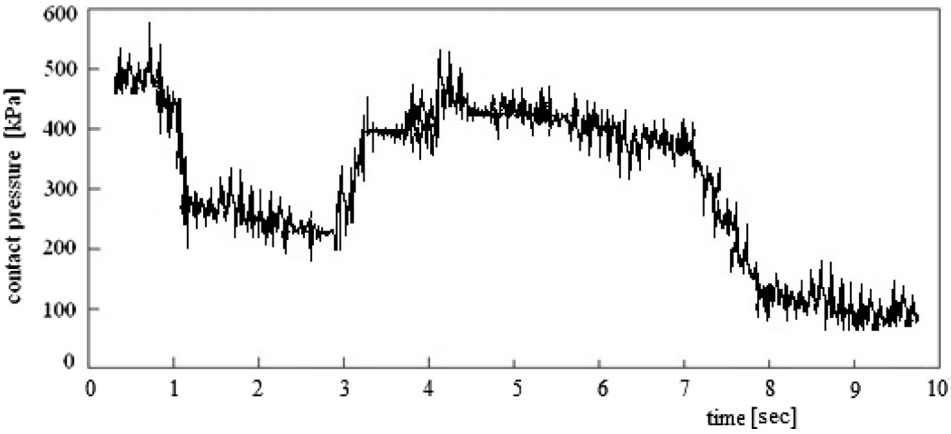

Fig. 15. Evolution in time of the maximum contact pressure in an arbitrary point of the contact patch.

normal forces as well as their geometric distributions in the random contact patches is made by taken account the inhomogeneities of the cross-sectional curves of off-roads before and after deformation, the contact between the tire and the road and the distribution of contact and friction forces in the contact paths.

The sonification is a multi-scale dynamic approach based on the 3D normal vibro-contact analysis and identification of the contact patches between tire and road. The road irregularities such as jump bumps, depressions, potholes, slopes, vertical upwards, lane grooves, rough obstacles are extracted from digital images. The sound is generated from images, possible in a bijective way, and tested to see whether they aid in the study of them, or not.

In order to show the efficiency of the sonification procedure and to verify the correctness of the results, we compare our results with other results from the literature obtained by other methods or by experiments.

The approach is exercised on two particular problems and results compare favorably to existing analytical and numerical solutions.

The road design algorithm can be adapted for a real-time sonification and admits a height accuracy because of exactly solvable equations or boundary conditions without uncertainties.

The sonification technique represents a useful multiscale analysis able to build a low-cost virtual reality environment with increased degrees of realism for driving simulators and higher user flexibility.

Acknowledgement

This research was elaborated through the PN-II-PT-PCCA-2011-3.1-0190 Project nr. 149/2012 of the National Authority for Scientific Research (ANCS, UEFISCDI), Romania. The authors acknowledge the similar and equal contributions to this article.

References

[1] P.W. Backs, Tyre/road contact measurements using pressure sensitive films, Technische Universiteit Eindhoven, Report DCT 2007-026, 2007, pp. 1–35.
[2] P. Barkan, Impact design, in: Mechanical Design and Systems Handbook, Section 31, McGraw-Hill, New York, 1974.
[3] E.J. Berger, Friction modeling for dynamic system simulation, Appl. Mech. Rev. 55 (2002) 535–577.
[4] T. Bonebright, P. Cook, J.H. Flowers, Sonification Report: Status of the Field and Research Agenda, Faculty Publications, Department of Psychology, Paper 444, 2010.
[5] D. Boediehn, K. Fritzsch, Vertical dynamics of an offroad race car (Motion solve), Motor Sport Altair MBD-Conference USA, 2009.
[6] R.M. Brach, Mechanical Impact Dynamics: Rigid Body Collisions, John Wiley and Sons, New York, 1991.
[7] C. Brişan, R.V. Vasiu, L. Munteanu, A modular road auto-generating algorithm for developing the road models for driving simulators, Transport. Res. Part C: Emerg. Technol. 26 (2013) 269–284.
[8] V. Chiroiu, D. Dumitriu, L. Solomon, On the nonlocal modeling of nanoindentation and nanocontacts, Research Trends in Mechanics, vol. 1, Publishing House of the Romanian Academy, 2007, pp. 33–54.
[9] D. Dumitriu, L. Munteanu, C. Brişan, V. Chiroiu, R.V. Vasiu, O. Melinte, V. Vlădăreanu, On the continuum modeling of the tire/ road dynamic contact, CMES: Comput. Model. Eng. Sci., Mater. Continua 94 (2) (2013) 159–173.
[10] D. Dumitriu, V. Chiroiu, On the dual equations in contact elasticity, in: Revue Roumaine des Sciences Techniques – Série de Mécanique Appliquée, 2006.
[11] S. Ferguson, W. Martens, D. Cabrera, Statistical sonification for exploratory data analysis, in: Thomas Hermann, Andy Hunt, John G. Neuhoff (Eds.), The Sonification Handbook, Logos Verlag, Berlin, Germany, 2011, pp. 176–196.
[12] A.A. Ferri, Friction damping and isolation systems, J. Mech. Des. 117 (1995) 196–206.
[13] Y.F. Gao, B.N. Lucas, J.C. Hay, W.C. Oliver, G.M. Pharr, Nanoscale incipient asperity sliding and interface micro-slip assessed by the measurement of tangential contact stiffness, Scripta Mater. 55 (2006) 653–656.
[14] M. Gardner, Piet Hein's Superellipse, Ch. 18 in Mathematical Carnival: A New Round-up of Tantalizers and Puzzles from Scientific American, Vintage, New York, 1977, pp. 240–254.
[15] G. Gilardi, I. Sharf, Literature survey of contact dynamics modeling, Mech. Mach. Theory 37 (2002) 1213–1239.

[16] D. Guo, Parameterized road databases for driving simulation, in: International Conference on Computer Science and Service System (CSSS), Nanjing, 27–29 June 2011, 2011, pp. 3976–3979.
[17] T. Hermann, Taxonomy and definitions for sonification and auditory display, in: Proceedings of the 14th International Conference on Auditory Display, Paris, France June 24–27, 2008.
[18] K.H. Hunt, F.R.E. Crossley, Coefficient of restitution interpreted as damping in vibroimpact, J. Appl. Mech. 42 (Series E) (1975) 440–445.
[19] H. Jalali, H. Ahmadian, F. Pourahmadian, Identification of micro-vibro-impacts at boundary condition of a nonlinear beam, Mech. Syst. Sig. Process. 25 (2011) 1073–1085.
[20] K.L. Johnson, Contact Mechanics, Cambridge University Press, Cambridge, 1985.
[21] K.L. Johnson, Adhesion and friction between a smooth elastic spherical asperity and a plane surface, Proc. Roy. Soc. London A 453 (1997) 163–179.
[22] D. Karnopp, Computer simulation of stick-slip friction in mechanical dynamic systems, J. Dyn. Syst. Meas. Contr. 107 (1985) 100–103.
[23] S.W. Kim, Contact Dynamics and Force Control of Flexible Multi-Body Systems Ph.D. Thesis, Department of Mechanical Engineering, McGill University, Montreal, 1999.
[24] D.A. Kessler, H. Levine, Fluctuation-induced diffusive instabilities, Nature 394 (1988) 556–558.
[25] G. Kramer, An introduction to auditory display, in: G. Kramer (Ed.), In Auditory Display, Addison-Wesley, Boston, MA, 1994, pp. 1–79.
[26] J. Li, E.J. Berger, A semi-analytical approach to three-dimensional normal contacts problems with friction, Comput. Mech. 30 (2003) 310–322.
[27] A. Licht, Sound Art, Beyond Music, Between Categories, Rizzoli International Publications Inc, New York, NY, 2007.
[28] A. Liggins, J. Stranart, J. Finlay, C. Rorabeck, Calibration and manipulation of data from fuji pressure-sensitive film, in: E. Little (Ed.), Experimental Mechanics – Technology Transfer Between High Tech Engineering and Biomechanics, Elsevier Science Publishers BV, 1992, pp. 61–70.
[29] C.T. Lim, W.J. Stronge, Oblique elastic–plastic impact between rough cylinders in plane strain, Int. J. Eng. Sci. 37 (1) (1999) 97–122.
[30] W. Luo, Wiener Chaos Expansion and Numerical Solutions of Stochastic Differential Equations PhD thesis, California Institute of technology, Pasadena, 2006.
[31] C.H. Menq, J. Bielak, J.H. Griffin, The influence of microslip on vibratory response, Part I: a new microslip model, J. Sound Vib. 107 (2) (1986) 279–293.
[32] L. Munteanu, V. Chiroiu, C. Brişan, D. Dumitriu, T. Sireteanu, S. Petre, On the 3D normal tire/off-road vibro-contact problem with friction, Mech. Syst. Sig. Process. 54–55 (2014) 377–393.
[33] L. Munteanu, C. Brisan, V. Chiroiu, Şt. Donescu, A 3D model for tire/road dynamic contact, Acta Technica Napocensis, Series: Appl. Math. Mech. 55 (3) (2012) 611–614.
[34] I.A. Shalimova, K.K. Sabelfeld, Stochastic polynomial chaos based algorithm for solving PDEs with random coefficients, Monte Carlo Methods and Applications, De Gruyter 20 (4) (2014) 279–289.
[35] T. Sireteanu, D. Gundisch, S. Paraian, Random Vibrations of Road Vehicle, Technical Publishing House, Bucharest, 1981.
[36] S. Shelley, M. Alonso, J. Hollowoof, M. Pettitt, S. Sharples, D. Hermes, A. Kohlrausch, Interactive sonification of curve shape and curvature data, in: M. Ercan Altinsoy, Ute Jekosch, Stephen Brewster (Eds.), Lecture Notes in Computer Science 5763, Haptic and Audio Interaction Design, 4th International Conference, HAID2009, Dresden, Germany, Sept 10–11, 2009, 2009, pp. 51–60.
[37] W.J. Stronge, Theoretical coefficient of restitution for planar impact of rough elasto-plastic bodies, Am. Soc. Mech. Eng. Appl. Mech. Div. AMD 205 (1995) 351–362.
[38] C. Tovar, G.J. Jimena, J.M. Cabanellas, C. Zoido, Modular technology in the modelling of large virtual environments in driving simulators, in: 12th International Conference on Computer Modelling and Simulation, Cambridge, 24–26 March 2010, 2010, pp. 468–473.
[39] J.W. Tukey, Exploratory Data Analysis, Addison-Wesley, Reading, Mass, 1977.
[40] J. Van Vliet, I. Sharf, O. Ma, Experimental validation of contact dynamics simulation of constrained robotic tasks, Int. J. Robot. Res. 19 (12) (2000) 1203–1217.
[41] R.V. Vasiu, C. Brisan, Aspects regarding modular road design in virtual reality, in: Proceedings of WINVR, Milan, 27–29 June 2011, 2011.
[42] R.V. Vasiu, O. Melinte, V. Vlădăreanu, D. Dumitriu, On the responseof the car from road disturbances, Romanian J. Tech. Sci. – Appl. Mech. 58 (3) (2013).
[43] M. Wiercigroch, Applied nonlinear dynamics of non-smooth mechanical systems, J. Braz. Soc. Mech. Sci. Eng. XXVIII (4) (2006) 519–526.
[44] X. Wan, D. Xiu, G.E. Karniadakis, Stochastic solutions for the two-dimensional advection-diffusion equation, SIAM J., Sci. Comp. 26 (2) (2004) 578–590.
[45] D. Xiu, D. Lucor, C.H. Su, G.E. Karniadakis, Stochastic modeling of flow-structure interactions using generalized polynomill chaos, Division of Applied Mathematics, Brown Unicversity, Providence, 2001.